Search for standard model Higgs boson production in association with a *W* boson using a neural network discriminant at CDF

T. Aaltonen,[24] J. Adelman,[14] T. Akimoto,[56] B. Álvarez González,[12,u] S. Amerio,[44b,44a] D. Amidei,[35] A. Anastassov,[39] A. Annovi,[20] J. Antos,[15] G. Apollinari,[18] A. Apresyan,[49] T. Arisawa,[58] A. Artikov,[16] W. Ashmanskas,[18] A. Attal,[4] A. Aurisano,[54] F. Azfar,[43] W. Badgett,[18] A. Barbaro-Galtieri,[29] V. E. Barnes,[49] B. A. Barnett,[26] P. Barria,[47c,47a] V. Bartsch,[31] G. Bauer,[33] P.-H. Beauchemin,[34] F. Bedeschi,[47a] D. Beecher,[31] S. Behari,[26] G. Bellettini,[47b,47a] J. Bellinger,[60] D. Benjamin,[17] A. Beretvas,[18] J. Beringer,[29] A. Bhatti,[51] M. Binkley,[18] D. Bisello,[44b,44a] I. Bizjak,[31,z] R. E. Blair,[2] C. Blocker,[7] B. Blumenfeld,[26] A. Bocci,[17] A. Bodek,[50] V. Boisvert,[50] G. Bolla,[49] D. Bortoletto,[49] J. Boudreau,[48] A. Boveia,[11] B. Brau,[11,b] A. Bridgeman,[25] L. Brigliadori,[6b,6a] C. Bromberg,[36] E. Brubaker,[14] J. Budagov,[16] H. S. Budd,[50] S. Budd,[25] S. Burke,[18] K. Burkett,[18] G. Busetto,[44b,44a] P. Bussey,[22] A. Buzatu,[34] K. L. Byrum,[2] S. Cabrera,[17,w] C. Calancha,[32] M. Campanelli,[36] M. Campbell,[35] F. Canelli,[14,18] A. Canepa,[46] B. Carls,[25] D. Carlsmith,[60] R. Carosi,[47a] S. Carrillo,[19,o] S. Carron,[34] B. Casal,[12] M. Casarsa,[18] A. Castro,[6b,6a] P. Catastini,[47c,47a] D. Cauz,[55b,55a] V. Cavaliere,[47c,47a] M. Cavalli-Sforza,[4] A. Cerri,[29] L. Cerrito,[31,q] S. H. Chang,[62] Y. C. Chen,[1] M. Chertok,[8] G. Chiarelli,[47a] G. Chlachidze,[18] F. Chlebana,[18] K. Cho,[62] D. Chokheli,[16] J. P. Chou,[23] G. Choudalakis,[33] S. H. Chuang,[53] K. Chung,[18,p] W. H. Chung,[60] Y. S. Chung,[50] T. Chwalek,[27] C. I. Ciobanu,[45] M. A. Ciocci,[47c,47a] A. Clark,[21] D. Clark,[7] G. Compostella,[44a] M. E. Convery,[18] J. Conway,[8] M. Cordelli,[20] G. Cortiana,[44b,44a] C. A. Cox,[8] D. J. Cox,[8] F. Crescioli,[47b,47a] C. Cuenca Almenar,[8,w] J. Cuevas,[12,u] R. Culbertson,[18] J. C. Cully,[35] D. Dagenhart,[18] M. Datta,[18] T. Davies,[22] P. de Barbaro,[50] S. De Cecco,[52a] A. Deisher,[29] G. De Lorenzo,[4] M. Dell'Orso,[47b,47a] C. Deluca,[4] L. Demortier,[51] J. Deng,[17] M. Deninno,[6a] P. F. Derwent,[18] A. Di Canto,[47b,47a] G. P. di Giovanni,[45] C. Dionisi,[52b,52a] B. Di Ruzza,[55b,55a] J. R. Dittmann,[5] M. D'Onofrio,[4] S. Donati,[47b,47a] P. Dong,[9] J. Donini,[44a] T. Dorigo,[44a] S. Dube,[53] J. Efron,[40] A. Elagin,[54] R. Erbacher,[8] D. Errede,[25] S. Errede,[25] R. Eusebi,[18] H. C. Fang,[29] S. Farrington,[43] W. T. Fedorko,[14] R. G. Feild,[61] M. Feindt,[27] J. P. Fernandez,[32] C. Ferrazza,[47d,47a] R. Field,[19] G. Flanagan,[49] R. Forrest,[8] M. J. Frank,[5] M. Franklin,[23] J. C. Freeman,[18] I. Furic,[19] M. Gallinaro,[52a] J. Galyardt,[13] F. Garberson,[11] J. E. Garcia,[21] A. F. Garfinkel,[49] P. Garosi,[47c,47a] K. Genser,[18] H. Gerberich,[25] D. Gerdes,[35] A. Gessler,[27] S. Giagu,[52b,52a] V. Giakoumopoulou,[3] P. Giannetti,[47a] K. Gibson,[48] J. L. Gimmell,[50] C. M. Ginsburg,[18] N. Giokaris,[3] M. Giordani,[55b,55a] P. Giromini,[20] M. Giunta,[47a] G. Giurgiu,[26] V. Glagolev,[16] D. Glenzinski,[18] M. Gold,[38] N. Goldschmidt,[19] A. Golossanov,[18] G. Gomez,[12] G. Gomez-Ceballos,[33] M. Goncharov,[33] O. González,[32] I. Gorelov,[38] A. T. Goshaw,[17] K. Goulianos,[51] A. Gresele,[44b,44a] S. Grinstein,[23] C. Grosso-Pilcher,[14] R. C. Group,[18] U. Grundler,[25] J. Guimaraes da Costa,[23] Z. Gunay-Unalan,[36] C. Haber,[29] K. Hahn,[33] S. R. Hahn,[18] E. Halkiadakis,[53] B.-Y. Han,[50] J. Y. Han,[50] F. Happacher,[20] K. Hara,[56] D. Hare,[53] M. Hare,[57] S. Harper,[43] R. F. Harr,[59] R. M. Harris,[18] M. Hartz,[48] K. Hatakeyama,[51] C. Hays,[43] M. Heck,[27] A. Heijboer,[46] J. Heinrich,[46] C. Henderson,[33] M. Herndon,[60] J. Heuser,[27] S. Hewamanage,[5] D. Hidas,[17] C. S. Hill,[11,d] D. Hirschbuehl,[27] A. Hocker,[18] S. Hou,[1] M. Houlden,[30] S.-C. Hsu,[29] B. T. Huffman,[43] R. E. Hughes,[40] U. Husemann,[61] M. Hussein,[36] J. Huston,[36] J. Incandela,[11] G. Introzzi,[47a] M. Iori,[52b,52a] A. Ivanov,[8] E. James,[18] D. Jang,[13] B. Jayatilaka,[17] E. J. Jeon,[62] M. K. Jha,[6a] S. Jindariani,[18] W. Johnson,[8] M. Jones,[49] K. K. Joo,[62] S. Y. Jun,[13] J. E. Jung,[62] T. R. Junk,[18] T. Kamon,[54] D. Kar,[19] P. E. Karchin,[59] Y. Kato,[42,n] R. Kephart,[18] W. Ketchum,[14] J. Keung,[46] V. Khotilovich,[54] B. Kilminster,[18] D. H. Kim,[62] H. S. Kim,[62] H. W. Kim,[62] J. E. Kim,[62] M. J. Kim,[20] S. B. Kim,[62] S. H. Kim,[56] Y. K. Kim,[14] N. Kimura,[56] L. Kirsch,[7] S. Klimenko,[19] B. Knuteson,[33] B. R. Ko,[17] K. Kondo,[58] D. J. Kong,[62] J. Konigsberg,[19] A. Korytov,[19] A. V. Kotwal,[17] M. Kreps,[27] J. Kroll,[46] D. Krop,[14] N. Krumnack,[5] M. Kruse,[17] V. Krutelyov,[11] T. Kubo,[56] T. Kuhr,[27] N. P. Kulkarni,[59] M. Kurata,[56] S. Kwang,[14] A. T. Laasanen,[49] S. Lami,[47a] S. Lammel,[18] M. Lancaster,[31] R. L. Lander,[8] K. Lannon,[40,t] A. Lath,[53] G. Latino,[47c,47a] I. Lazzizzera,[44b,44a] T. LeCompte,[2] E. Lee,[54] H. S. Lee,[14] S. W. Lee,[54,v] S. Leone,[47a] J. D. Lewis,[18] C.-S. Lin,[29] J. Linacre,[43] M. Lindgren,[18] E. Lipeles,[46] A. Lister,[8] D. O. Litvintsev,[18] C. Liu,[48] T. Liu,[18] N. S. Lockyer,[46] A. Loginov,[61] M. Loreti,[44b,44a] L. Lovas,[15] D. Lucchesi,[44b,44a] C. Luci,[52b,52a] J. Lueck,[27] P. Lujan,[29] P. Lukens,[18] G. Lungu,[51] L. Lyons,[43] J. Lys,[29] R. Lysak,[15] D. MacQueen,[34] R. Madrak,[18] K. Maeshima,[18] K. Makhoul,[33] T. Maki,[24] P. Maksimovic,[26] S. Malde,[43] S. Malik,[31] G. Manca,[30,f] A. Manousakis-Katsikakis,[3] F. Margaroli,[49] C. Marino,[27] C. P. Marino,[25] A. Martin,[61] V. Martin,[22,l] M. Martínez,[4] R. Martínez-Ballarín,[32] T. Maruyama,[56] P. Mastrandrea,[52a] T. Masubuchi,[56] M. Mathis,[26] M. E. Mattson,[59] P. Mazzanti,[6a] K. S. McFarland,[50] P. McIntyre,[54] R. McNulty,[30,k] A. Mehta,[30] P. Mehtala,[24] A. Menzione,[47a] P. Merkel,[49] C. Mesropian,[51] T. Miao,[18] N. Miladinovic,[7] R. Miller,[36] C. Mills,[23] M. Milnik,[27] A. Mitra,[1] G. Mitselmakher,[19] H. Miyake,[56] N. Moggi,[6a] M. N. Mondragon,[18,o] C. S. Moon,[62] R. Moore,[18] M. J. Morello,[47a] J. Morlock,[27] P. Movilla Fernandez,[18] J. Mülmenstädt,[29] A. Mukherjee,[18] Th. Muller,[27] R. Mumford,[26] P. Murat,[18] M. Mussini,[6b,6a] J. Nachtman,[18,p] Y. Nagai,[56] A. Nagano,[56] J. Naganoma,[56]

K. Nakamura,[56] I. Nakano,[41] A. Napier,[57] V. Necula,[17] J. Nett,[60] C. Neu,[46,x] M. S. Neubauer,[25] S. Neubauer,[27] J. Nielsen,[29,h] L. Nodulman,[2] M. Norman,[10] O. Norniella,[25] E. Nurse,[31] L. Oakes,[43] S. H. Oh,[17] Y. D. Oh,[62] I. Oksuzian,[19] T. Okusawa,[42] R. Orava,[24] K. Osterberg,[24] S. Pagan Griso,[44b,44a] E. Palencia,[18] V. Papadimitriou,[18] A. Papaikonomou,[27] A. A. Paramonov,[14] B. Parks,[40] S. Pashapour,[34] J. Patrick,[18] G. Pauletta,[55b,55a] M. Paulini,[13] C. Paus,[33] T. Peiffer,[27] D. E. Pellett,[8] A. Penzo,[55a] T. J. Phillips,[17] G. Piacentino,[47a] E. Pianori,[46] L. Pinera,[19] K. Pitts,[25] C. Plager,[9] L. Pondrom,[60] O. Poukhov,[16,a] N. Pounder,[43] F. Prakoshyn,[16] A. Pronko,[18] J. Proudfoot,[2] F. Ptohos,[18,j] E. Pueschel,[13] G. Punzi,[47b,47a] J. Pursley,[60] J. Rademacker,[43,d] A. Rahaman,[48] V. Ramakrishnan,[60] N. Ranjan,[49] I. Redondo,[32] P. Renton,[43] M. Renz,[27] M. Rescigno,[52a] S. Richter,[27] F. Rimondi,[6b,6a] L. Ristori,[47a] A. Robson,[22] T. Rodrigo,[12] T. Rodriguez,[46] E. Rogers,[25] S. Rolli,[57] R. Roser,[18] M. Rossi,[55a] R. Rossin,[11] P. Roy,[34] A. Ruiz,[12] J. Russ,[13] V. Rusu,[18] B. Rutherford,[18] H. Saarikko,[24] A. Safonov,[54] W. K. Sakumoto,[50] O. Saltó,[4] L. Santi,[55b,55a] S. Sarkar,[52b,52a] L. Sartori,[47a] K. Sato,[18] A. Savoy-Navarro,[45] P. Schlabach,[18] A. Schmidt,[27] E. E. Schmidt,[18] M. A. Schmidt,[14] M. P. Schmidt,[61,a] M. Schmitt,[39] T. Schwarz,[8] L. Scodellaro,[12] A. Scribano,[47c,47a] F. Scuri,[47a] A. Sedov,[49] S. Seidel,[38] Y. Seiya,[42] A. Semenov,[16] L. Sexton-Kennedy,[18] F. Sforza,[47a] A. Sfyrla,[25] S. Z. Shalhout,[59] T. Shears,[30] P. F. Shepard,[48] M. Shimojima,[56,s] S. Shiraishi,[14] M. Shochet,[14] Y. Shon,[60] I. Shreyber,[37] P. Sinervo,[34] A. Sisakyan,[16] A. J. Slaughter,[18] J. Slaunwhite,[40] K. Sliwa,[57] J. R. Smith,[8] F. D. Snider,[18] R. Snihur,[34] A. Soha,[8] S. Somalwar,[53] V. Sorin,[36] T. Spreitzer,[34] P. Squillacioti,[47c,47a] M. Stanitzki,[61] R. St. Denis,[22] B. Stelzer,[34] O. Stelzer-Chilton,[34] D. Stentz,[39] J. Strologas,[38] G. L. Strycker,[35] J. S. Suh,[62] A. Sukhanov,[19] I. Suslov,[16] T. Suzuki,[56] A. Taffard,[25,g] R. Takashima,[41] Y. Takeuchi,[56] R. Tanaka,[41] M. Tecchio,[35] P. K. Teng,[1] K. Terashi,[51] J. Thom,[18,i] A. S. Thompson,[22] G. A. Thompson,[25] E. Thomson,[46] P. Tipton,[61] P. Ttito-Guzmán,[32] S. Tkaczyk,[18] D. Toback,[54] S. Tokar,[15] K. Tollefson,[36] T. Tomura,[56] D. Tonelli,[18] S. Torre,[20] D. Torretta,[18] P. Totaro,[55b,55a] S. Tourneur,[45] M. Trovato,[47d,47a] S.-Y. Tsai,[1] Y. Tu,[46] N. Turini,[47c,47a] F. Ukegawa,[56] S. Vallecorsa,[21] N. van Remortel,[24,c] A. Varganov,[35] E. Vataga,[47d,47a] F. Vázquez,[19,o] G. Velev,[18] C. Vellidis,[3] M. Vidal,[32] R. Vidal,[18] I. Vila,[12] R. Vilar,[12] T. Vine,[31] M. Vogel,[38] I. Volobouev,[29,v] G. Volpi,[47b,47a] P. Wagner,[46] R. G. Wagner,[2] R. L. Wagner,[18] W. Wagner,[27,y] J. Wagner-Kuhr,[27] T. Wakisaka,[42] R. Wallny,[9] S. M. Wang,[1] A. Warburton,[34] D. Waters,[31] M. Weinberger,[54] J. Weinelt,[27] W. C. Wester III,[18] B. Whitehouse,[57] D. Whiteson,[46,g] A. B. Wicklund,[2] E. Wicklund,[18] S. Wilbur,[14] G. Williams,[34] H. H. Williams,[46] P. Wilson,[18] B. L. Winer,[40] P. Wittich,[18,i] S. Wolbers,[18] C. Wolfe,[14] T. Wright,[35] X. Wu,[21] F. Würthwein,[10] S. Xie,[33] A. Yagil,[10] K. Yamamoto,[42] J. Yamaoka,[17] U. K. Yang,[14,r] Y. C. Yang,[62] W. M. Yao,[29] G. P. Yeh,[18] K. Yi,[18,p] J. Yoh,[18] K. Yorita,[58] T. Yoshida,[42,m] G. B. Yu,[50] I. Yu,[62] S. S. Yu,[18] J. C. Yun,[18] L. Zanello,[52b,52a] A. Zanetti,[55a] X. Zhang,[25] Y. Zheng,[9,e] and S. Zucchelli[6b,6a]

(CDF Collaboration)

[1]*Institute of Physics, Academia Sinica, Taipei, Taiwan 11529, Republic of China*
[2]*Argonne National Laboratory, Argonne, Illinois 60439*
[3]*University of Athens, 157 71 Athens, Greece*
[4]*Institut de Fisica d'Altes Energies, Universitat Autonoma de Barcelona, E-08193, Bellaterra (Barcelona), Spain*
[5]*Baylor University, Waco, Texas 76798*
[6a]*Istituto Nazionale di Fisica Nucleare Bologna, I-40127 Bologna, Italy*
[6b]*University of Bologna, I-40127 Bologna, Italy*
[7]*Brandeis University, Waltham, Massachusetts 02254*
[8]*University of California, Davis, Davis, California 95616*
[9]*University of California, Los Angeles, Los Angeles, California 90024*
[10]*University of California, San Diego, La Jolla, California 92093*
[11]*University of California, Santa Barbara, Santa Barbara, California 93106*
[12]*Instituto de Fisica de Cantabria, CSIC-University of Cantabria, 39005 Santander, Spain*
[13]*Carnegie Mellon University, Pittsburgh, Pennsylvania 15213*
[14]*Enrico Fermi Institute, University of Chicago, Chicago, Illinois 60637*
[15]*Comenius University, 842 48 Bratislava, Slovakia; Institute of Experimental Physics, 040 01 Kosice, Slovakia*
[16]*Joint Institute for Nuclear Research, RU-141980 Dubna, Russia*
[17]*Duke University, Durham, North Carolina 27708*
[18]*Fermi National Accelerator Laboratory, Batavia, Illinois 60510*
[19]*University of Florida, Gainesville, Florida 32611*
[20]*Laboratori Nazionali di Frascati, Istituto Nazionale di Fisica Nucleare, I-00044 Frascati, Italy*
[21]*University of Geneva, CH-1211 Geneva 4, Switzerland*
[22]*Glasgow University, Glasgow G12 8QQ, United Kingdom*
[23]*Harvard University, Cambridge, Massachusetts 02138*

[24]Division of High Energy Physics, Department of Physics, University of Helsinki and Helsinki Institute of Physics, FIN-00014, Helsinki, Finland
[25]University of Illinois, Urbana, Illinois 61801
[26]The Johns Hopkins University, Baltimore, Maryland 21218
[27]Institut für Experimentelle Kernphysik, Universität Karlsruhe, 76128 Karlsruhe, Germany
[28]Center for High Energy Physics: Kyungpook National University, Daegu 702-701, Korea; Seoul National University, Seoul 151-742, Korea; Sungkyunkwan University, Suwon 440-746, Korea; Korea Institute of Science and Technology Information, Daejeon, 305-806, Korea; Chonnam National University, Gwangju, 500-757, Korea; Chonbuk National University, Jeonju 561-756, Korea
[29]Ernest Orlando Lawrence Berkeley National Laboratory, Berkeley, California 94720
[30]University of Liverpool, Liverpool L69 7ZE, United Kingdom
[31]University College London, London WC1E 6BT, United Kingdom
[32]Centro de Investigaciones Energeticas Medioambientales y Tecnologicas, E-28040 Madrid, Spain
[33]Massachusetts Institute of Technology, Cambridge, Massachusetts 02139
[34]Institute of Particle Physics: McGill University, Montréal, Québec, Canada H3A 2T8; Simon Fraser University, Burnaby, British Columbia, Canada V5A 1S6; University of Toronto, Toronto, Ontario, Canada M5S 1A7; and TRIUMF, Vancouver, British Columbia, Canada V6T 2A3
[35]University of Michigan, Ann Arbor, Michigan 48109
[36]Michigan State University, East Lansing, Michigan 48824
[37]Institution for Theoretical and Experimental Physics, ITEP, Moscow 117259, Russia
[38]University of New Mexico, Albuquerque, New Mexico 87131
[39]Northwestern University, Evanston, Illinois 60208
[40]The Ohio State University, Columbus, Ohio 43210
[41]Okayama University, Okayama 700-8530, Japan
[42]Osaka City University, Osaka 588, Japan
[43]University of Oxford, Oxford OX1 3RH, United Kingdom
[44a]Istituto Nazionale di Fisica Nucleare, Sezione di Padova-Trento, I-35131 Padova, Italy
[44b]University of Padova, I-35131 Padova, Italy
[45]LPNHE, Universite Pierre et Marie Curie/IN2P3-CNRS, UMR7585, Paris, F-75252 France
[46]University of Pennsylvania, Philadelphia, Pennsylvania 19104
[47a]Istituto Nazionale di Fisica Nucleare Pisa, I-56127 Pisa, Italy
[47b]University of Pisa, I-56127 Pisa, Italy
[47c]University of Siena, I-56127 Pisa, Italy
[47d]Scuola Normale Superiore, I-56127 Pisa, Italy
[48]University of Pittsburgh, Pittsburgh, Pennsylvania 15260
[49]Purdue University, West Lafayette, Indiana 47907
[50]University of Rochester, Rochester, New York 14627
[51]The Rockefeller University, New York, New York 10021
[52a]Istituto Nazionale di Fisica Nucleare, Sezione di Roma 1, I-00185 Roma, Italy

[a]Deceased.
[b]Visitor from University of Massachusetts Amherst, Amherst, MA 01003.
[c]Visitor from Universiteit Antwerpen, B-2610 Antwerp, Belgium.
[d]Visitor from University of Bristol, Bristol BS8 1TL, United Kingdom.
[e]Visitor from Chinese Academy of Sciences, Beijing 100864, China.
[f]Visitor from Istituto Nazionale di Fisica Nucleare, Sezione di Cagliari, 09042 Monserrato (Cagliari), Italy.
[g]Visitor from University of California Irvine, Irvine, CA 92697.
[h]Visitor from University of California Santa Cruz, Santa Cruz, CA 95064.
[i]Visitor from Cornell University, Ithaca, NY 14853.
[j]Visitor from University of Cyprus, Nicosia CY-1678, Cyprus.
[k]Visitor from University College Dublin, Dublin 4, Ireland.
[l]Visitor from University of Edinburgh, Edinburgh EH9 3JZ, United Kingdom.
[m]Visitor from University of Fukui, Fukui City, Fukui Prefecture, Japan 910-0017.
[n]Visitor from Kinki University, Higashi-Osaka City, Japan 577-8502.
[o]Visitor from Universidad Iberoamericana, Mexico D.F., Mexico.
[p]Visitor from University of Iowa, Iowa City, IA 52242.
[q]Visitor from Queen Mary, University of London, London, E1 4NS, United Kingdom.
[r]Visitor from University of Manchester, Manchester M13 9PL, United Kingdom.
[s]Visitor from Nagasaki Institute of Applied Science, Nagasaki, Japan.
[t]Visitor from University of Notre Dame, Notre Dame, IN 46556.
[u]Visitor from University de Oviedo, E-33007 Oviedo, Spain.
[v]Visitor from Texas Tech University, Lubbock, TX 79609.
[w]Visitor from IFIC(CSIC-Universitat de Valencia), 46071 Valencia, Spain.
[x]Visitor from University of Virginia, Charlottesville, VA 22904.
[y]Visitor from Bergische Universität Wuppertal, 42097 Wuppertal, Germany.
[z]On leave from J. Stefan Institute, Ljubljana, Slovenia.

[52b]*Sapienza Università di Roma, I-00185 Roma, Italy*
[53]*Rutgers University, Piscataway, New Jersey 08855*
[54]*Texas A&M University, College Station, Texas 77843*
[55a]*Istituto Nazionale di Fisica Nucleare Trieste/Udine, I-34100 Trieste, Italy*
[55b]*University of Trieste/Udine, I-33100 Udine, Italy*
[56]*University of Tsukuba, Tsukuba, Ibaraki 305, Japan*
[57]*Tufts University, Medford, Massachusetts 02155*
[58]*Waseda University, Tokyo 169, Japan*
[59]*Wayne State University, Detroit, Michigan 48201*
[60]*University of Wisconsin, Madison, Wisconsin 53706*
[61]*Yale University, New Haven, Connecticut 06520*
[62]*Center for High Energy Physics: Kyungpook National University, Daegu 702-701, Korea; Seoul National University, Seoul 151-742, Korea; Sungkyunkwan University, Suwon 440-746, Korea; Korea Institute of Science and Technology Information, Daejeon, 305-806, Korea; Chonnam National University, Gwangju, 500-757, Korea*

(Received 20 May 2009; published 14 July 2009)

We present a search for standard model Higgs boson production in association with a W boson in proton-antiproton collisions ($p\bar{p} \to W^{\pm}H \to \ell\nu b\bar{b}$) at a center of mass energy of 1.96 TeV. The search employs data collected with the CDF II detector that correspond to an integrated luminosity of approximately 1.9 fb^{-1}. We select events consistent with a signature of a single charged lepton ($e^{\pm}/\mu^{\pm}$), missing transverse energy, and two jets. Jets corresponding to bottom quarks are identified with a secondary vertex tagging method, a jet probability tagging method, and a neural network filter. We use kinematic information in an artificial neural network to improve discrimination between signal and background compared to previous analyses. The observed number of events and the neural network output distributions are consistent with the standard model background expectations, and we set 95% confidence level upper limits on the production cross section times branching fraction ranging from 1.2 to 1.1 pb or 7.5 to 102 times the standard model expectation for Higgs boson masses from 110 to 150 GeV/c^2, respectively.

DOI: 10.1103/PhysRevD.80.012002 PACS numbers: 13.85.Rm, 14.80.Bn

I. INTRODUCTION

Standard electroweak theory predicts a single fundamental scalar particle, the Higgs boson, which arises as a result of spontaneous electroweak symmetry breaking [1]. However, the Higgs boson is the only fundamental standard model particle which has not been directly observed by experiments. The current experimental constraint on the Higgs boson mass, $m_H > 114.4$ GeV/c^2 at 95% confidence level (C.L.), comes from direct Higgs boson searches at LEP experiments [2]. Global fits to electroweak measurements exclude masses above 154 GeV/c^2 at 95% confidence level [3].

At the Tevatron $p\bar{p}$ collider at Fermilab, the next-to-leading-order (NLO) Higgs boson production cross section is about 10 times larger for gluon fusion than for WH associated production, and the cross section for WH is about twice that of ZH [4]. The Higgs boson decay branching fraction is dominated by $H \to b\bar{b}$ for $m_H < 135$ GeV/c^2 and by $H \to W^+W^-$ for $m_H > 135$ GeV/c^2 [5]. Background $b\bar{b}$ production processes have QCD cross sections at least 4 orders of magnitude greater than that of Higgs boson production [6], and this renders searches in the $gg \to H \to b\bar{b}$ channel nonviable. Requiring the leptonic decay of the associated W boson reduces the huge $b\bar{b}$ background rate. As a result, $WH \to \ell\nu b\bar{b}$ is one of the most favorable channels for a low mass Higgs boson search,[1] and it forms an important component of the combined search for the Higgs boson at the Tevatron.

Searches for $WH \to \ell\nu b\bar{b}$ at $\sqrt{s} = 1.96$ TeV have been most recently reported by CDF [7,8] and D0 [9] using data corresponding to an integrated luminosity of 955 pb^{-1} and 440 pb^{-1}, respectively. In this paper, we present an update on the search for $WH \to \ell\nu b\bar{b}$ production at CDF using about 1.9 fb^{-1} of data and improved analysis techniques. The b hadrons which arise from $b\bar{b}$ quark pairs in this final state can be identified through special algorithms based on the tracking information for particles within hadronic jets, a procedure known as b-tagging. We have optimized the b-tagging algorithms to increase the acceptance for double b-tagged events. In addition we increase the signal acceptance by including the electrons going into the forward region of the detector and introduce a multivariate discriminant technique using a neural network (NN) to reduce large background contamination after the event selection.

The paper is organized as follows. Section II describes the CDF II detector. The event selection criteria are explained in Sec. III. In Sec. IV the b-tagging algorithms

[1]In this paper, lepton (ℓ) denotes electron ($e^{\pm}$) or muon ($\mu^{\pm}$), and neutrino (ν) denotes electron neutrino (ν_e) or muon neutrino (ν_μ) or their antiparticles.

SECVTX [10], neural net b-tagging filter, and jet probability [11] are discussed in detail. Contributions from the standard model (SM) background in the $WH \to \ell\nu b\bar{b}$ channel are calculated in Sec. V for various sources. In Sec. VI, signal acceptance and systematic uncertainties are estimated. The neural network discriminant technique is described in Sec. VII. The results and their statistical interpretation are presented in Sec. VIII. Finally, our conclusions are presented in Sec. IX.

II. CDF II DETECTOR

The CDF II detector [12] geometry is described using a cylindrical coordinate system. The z-axis follows the proton direction, and the polar angle θ is usually expressed through the pseudorapidity $\eta = -\ln(\tan(\theta/2))$. The detector is approximately symmetric in η and in the azimuthal angle ϕ. The transverse energy is defined as $E_T = E\sin\theta$, and the transverse momentum $p_T = p\sin\theta$.

Charged particles are tracked by a system of silicon microstrip detectors and a large open cell drift chamber in the region $|\eta| \leq 2.0$ and $|\eta| \leq 1.0$, respectively. The tracking detectors are immersed in a 1.4 T solenoidal magnetic field aligned coaxially with the incoming beams, allowing measurement of charged particle momentum transverse to the beamline (p_T).

The transverse momentum resolution is measured to be $\delta p_T/p_T \approx 0.07\% \cdot p_T$ (GeV) for the combined tracking system. The resolution on the track impact parameter (d_0), the distance from the beamline axis to the track at the track's closest approach in the transverse plane, is $\sigma(d_0) \approx 40\ \mu$m, of which about 30 μm is due to the transverse size of the Tevatron beam itself.

Outside of the tracking systems and the solenoid, segmented calorimeters with projective tower geometry are used to reconstruct electromagnetic showers and hadronic jets [13–15] over the pseudorapidity range $|\eta| < 3.6$. A transverse energy is measured in each calorimeter tower where the polar angle (θ) is calculated using the measured z position of the event vertex and the tower location.

Contiguous groups of calorimeter towers with signals are identified and summed together into an energy cluster. Electron candidates are identified in the central electromagnetic calorimeter (CEM) or in the forward, known as the plug, electromagnetic calorimeter (PEM) as isolated, mostly electromagnetic clusters that match a track in the pseudorapidity range $|\eta| < 1.1$ and $1.1 < |\eta| < 2.0$, respectively. The electron transverse energy is reconstructed from the electromagnetic cluster with a precision $\sigma(E_T)/E_T \approx 13.5\%/\sqrt{E_T(\mathrm{GeV})} \oplus 2\%$ for central electrons [13] and $\sigma(E_T)/E_T = 16.0\%/\sqrt{E_T(\mathrm{GeV})} \oplus 2\%$ for plug electrons. Jets are identified as a group of electromagnetic (EM) and hadronic (HAD) calorimeter clusters which fall within a cone of radius $\Delta R \approx \sqrt{(\Delta\phi)^2 + (\Delta\eta)^2} \leq 0.4$ units around a high-E_T seed cluster [16]. Jet energies are corrected for calorimeter nonlinearity, losses in the gaps between towers and multiple primary interactions. The jet energy resolution is approximately $\sigma(E_T) \approx [0.1E_T + 1.0\ \mathrm{GeV}]$ [17].

Muon candidates are detected in three separate subdetectors. After at least five interaction lengths in the calorimeter, the large angle muons first encounter four layers of planar drift chambers (CMU), capable of detecting muons with $p_T > 1.4$ GeV/c [18]. Four additional layers of planar drift chambers (CMP) behind another 60 cm of steel detect muons with $p_T > 2.8$ GeV/c [19]. These two systems cover the same central pseudorapidity region with $|\eta| \leq 0.6$. Muons that exit the calorimeters at $0.6 \leq |\eta| \leq 1.0$ are detected by the CMX system of four drift layers. Muon candidates are then identified as isolated tracks which extrapolate to line segments or "stubs" in the muon subdetectors. A track that is linked to both CMU and CMP stubs is called a CMUP muon.

The missing transverse energy ($\not\!\!E_T$) is a reconstructed quantity that is defined as the absolute value of the opposite of the vector sum of all calorimeter tower energy depositions projected on the transverse plane. It is often used as a measure of the sum of the transverse momenta of the particles that escape detection, most notably neutrinos. To be more readily interpretable as such, the raw $\not\!\!E_T$ vector is adjusted for corrected jet energies and the muon momentum is also added for any minimum ionizing high-p_T muon found in the event.

Muon and electron candidates used in this analysis are identified during data taking with the CDF trigger system, a three-level filter, with tracking information available at the first level [20]. Events used in this analysis have all passed the high-energy electron or muon trigger selection. The first stage of the central electron trigger (CEM) requires a track with $p_T > 8$ GeV/c pointing to a tower with $E_T > 8$ GeV and $E_{\mathrm{HAD}}/E_{\mathrm{EM}} < 0.125$. As appropriate for selecting W-decay electrons, the plug electron trigger (MET + PEM) requires a tower with $E_T > 8$ GeV, $E_{\mathrm{HAD}}/E_{\mathrm{EM}} < 0.125$ and the missing transverse energy $\not\!\!E_T > 15$ GeV. The first stage of the muon trigger requires a track with $p_T > 4$ GeV/c (CMUP) or 8 GeV/c (CMX) pointing to a muon stub. A complete lepton reconstruction is performed online in the final trigger stage, where we require $E_T > 18$ GeV for central electrons (CEM), $E_T > 18$ GeV and $\not\!\!E_T > 20$ GeV for plug electron (MET + PEM) and $p_T > 18$ GeV/c for muons (CMUP, CMX).

III. EVENT SELECTION

The results presented here use data collected between February 2002 and May 2007. The data collected using the CEM, CMUP and MET + PEM triggers correspond to 1.92 ± 0.12 fb^{-1} of integrated luminosity, while the data from the CMX trigger corresponds to 1.88 ± 0.11 fb^{-1}.

The observable final state from the $WH \to \ell\nu b\bar{b}$ signal consists of two b-jets from Higgs decay, while the decay of

W yields the high-p_T lepton and large missing transverse energy from the neutrino. Therefore events are considered as WH candidates only if they have exactly one lepton candidate [21], with $E_T > 20$ GeV for electrons or $p_T > 20$ GeV/c for muons. Because the lepton from a leptonic W decay is well-isolated from the rest of event, the cone of $\Delta R = 0.4$ surrounding the lepton is required to contain less than 10% of the lepton energy. A primary event vertex position is calculated by fitting a subset of particle tracks that are consistent with having come from the beamline. The closest distance z_0 along the beam line between the primary event vertex and the lepton track must be less than 5 cm to ensure the lepton and the jets come from the same hard interaction. Some leptonic Z decays would mimic the single-lepton signature if one of the leptons is missed. Therefore Z boson candidate events are rejected if a track, an EM cluster or a jet together with the primary lepton form an invariant mass between 76 and 106 GeV/c^2. The selected events are required to have $\not\!\!E_T$ greater than 20 GeV, to be consistent with the presence of a neutrino from W decay.

In the plug region, we also require a high-p_T isolated lepton candidate with $E_T > 20$ GeV, with the same selection criteria as for the central region. In addition, because the background contamination from multijet processes is higher in the forward region, we impose stricter criteria on the missing transverse energy, which improves the rejection of hadronic background events by a factor of 4 while only reducing the signal efficiency by 20%. We require that $\mathrm{MET_{sig}} > 2$, $\not\!\!E_T > 25$ GeV and $\not\!\!E_T > 45$ GeV when the $\not\!\!E_T$ is pointing close to a jet, and large transverse mass of the reconstructed W, $M_T(W) > 20$ GeV/c^2. Here, $\mathrm{MET_{sig}}$ is defined as the ratio of $\not\!\!E_T$ to the square root of a weighted sum of jet E_T with factors correlated with mismeasurement, such as angles between the $\not\!\!E_T$ and the jet and size of jet energy corrections [22], and $M_T(W)$ is defined as follows:

$$M_T(W) = \sqrt{2(p_T^{\mathrm{lep}} \not\!\!E_T - \vec{p}_T^{\,\mathrm{lep}} \cdot \vec{\not\!\!E}_T)}. \quad (1)$$

The WH signal includes two jets originating from $H \to b\bar{b}$ decays; these jets are expected to have large transverse energy. The jets are required to be in the pseudorapidity range covered by the silicon detector so that secondary vertices from b decays can be reconstructed. Specifically, we require the jets to satisfy $E_T > 20$ GeV and $|\eta| < 2.0$ and use loose jets ($E_T > 12$ GeV and $|\eta| < 2.4$) as input for the neural network discriminant discussed in Sec. VII. The search for $WH \to \ell\nu b\bar{b}$ is performed in the sample of events with $W +$ exactly 2 jets; however, samples of events with $W + 1$, 3, ≥ 4 jets are used to cross-check the background modeling.

To increase the signal purity of the $W + 2$ jets events, at least one jet must be b-tagged by the SECVTX algorithm as explained in the subsequent sections. Three exclusive b-tagged event categories are considered. The first category (ST + ST) is for events where there are two SECVTX b-tagged jets. The second category (ST + JP) consists of events where only one of the jets is b-tagged by the SECVTX and the second jet is b-tagged by jet probability. The third category (ST with NN filter) contains events where only one of the jets is b-tagged by the SECVTX and also passes the neural network b-tagging filter.

These three categories are selected exclusively and the tightest ST + ST category is preferentially selected. Subsequently the ST + JP category is considered if the ST + ST selection failed and finally ST with NN filter category is considered if both double b-tagged selections failed.

IV. *b* JET IDENTIFICATION ALGORITHMS

Multijet final states have dominant contributions from QCD light-flavor jet production, but the standard model Higgs boson decays predominantly to bottom quark pairs. Correctly identifying the b quark jets helps to remove most of the QCD background.

The b-quark has a relatively long lifetime, and b hadrons formed during the hadronization of the initial b quark can travel a significant distance before decaying into a collection of lighter hadrons. Jets containing a b-quark decay can be reconstructed by identifying tracks significantly displaced from the $p\bar{p}$ interaction point (primary vertex).

In this analysis, we employ three b-identification algorithms to optimize the selection of b-quark jets.

A. Secondary vertex *b*-tagging

The SECVTX b-tagging algorithm is applied to each jet in the event, using only the tracks which are within η-ϕ distance of $\Delta R = 0.4$ of the jet direction. Displaced tracks in jets are used for the SECVTX reconstruction and are distinguished by a large impact parameter significance ($|d_0/\sigma_{d_0}|$), where d_0 and σ_{d_0} are the impact parameter and the total uncertainty from tracking and beam position measurements, respectively. Secondary vertices are reconstructed with a two-pass approach which tests for high-quality vertices in the first pass and allows lower-quality vertices in the second pass. In pass 1, at least three tracks are required to pass loose selection criteria ($p_T > 0.5$ GeV/c, $|d_0/\sigma_{d_0}| > 2.0$), and a secondary vertex is fit from the selected tracks. One of the tracks used in the reconstruction is required to have $p_T > 1.0$ GeV/c. If pass 1 fails, then a vertex is sought in pass 2 from at least two tracks satisfying tight selection criteria ($p_T > 1.0$ GeV/c, $|d_0/\sigma_{d_0}| > 3.5$ and one of the pass 2 tracks must have $p_T > 1.5$ GeV/c). If either pass is successful, the transverse distance (L_{xy}) from the primary vertex of the event is calculated along with the associated uncertainty. This uncertainty $\sigma_{L_{xy}}$ includes the uncertainty on the primary vertex position. Finally jets are tagged positively or negatively depending on the L_{xy} significance ($L_{xy}/\sigma_{L_{xy}}$):

$$L_{xy}/\sigma_{L_{xy}} \geq 7.5 \qquad \text{(positive tag)} \tag{2}$$

$$L_{xy}/\sigma_{L_{xy}} \leq -7.5 \qquad \text{(negative tag).} \tag{3}$$

This value has been tuned for optimum efficiency and purity in simulated b-jet samples from decays of top quarks. The energy spectrum for those jets is similar to the spectrum for b jets from decays of Higgs bosons.

The sign of L_{xy} indicates the position of the secondary vertex with respect to the primary vertex along the direction of the jet. If the angle between the jet axis and the vector pointing from the primary vertex to the secondary vertex is less than $\pi/2$, L_{xy} is positively defined; otherwise, it is negative. If L_{xy} is positive, the secondary vertex points towards the direction of the jet, as in true b hadron decays. For negative L_{xy} the secondary vertex points away from the jet; this may happen as a result of mismeasured tracks. In order to reject secondary vertices due to material interaction, the algorithm vetoes two-track vertices found between 1.2 and 1.5 cm from the center of the silicon detector (the inner radius of the beampipe and the outer radius of the innermost silicon layer being within this range). All vertices more than 2.5 cm from the center are rejected because b-jets in WH events travel 3.5 mm on average.

The negative tags are useful for evaluating the rate of false positive tags, which are identified as ''mistags'' in the background estimates. Mismeasurements are expected to occur randomly; therefore the L_{xy} distribution of fake tags is expected to be symmetric around zero. Simulated events are used to correct a small asymmetry due to true long-lived particles in light-flavor jets and to interactions in the detector material.

The efficiency for identifying a secondary vertex is different in simulation and data. We measure an efficiency correction factor, which is defined as the ratio of the observed to the simulated efficiencies, to be 0.95 ± 0.04 in a sample of high-E_T jets enriched in b jets by requiring a soft lepton ($p_T > 8$ GeV/c) from semileptonic heavy quark decays [10].

B. Neural network b-tagging filter

The sample tagged by the SECVTX algorithm still has significant contamination from falsely-tagged light-flavor or gluon jets and the misidentification of c quarks as b-jets [23]. This search uses a multivariate neural network (NN) technique to improve the SECVTX tagging purity [7,8].

The neural network used in this article employs the JETNET [24] package. The tagger is designed with two neural networks in series. The $b - l$ network is trained to separate b-jets from light-quark jets (l-jets), and the $b - c$ network is trained to separate b-jets from c-jets. Jets that pass a cut on both of the neural network outputs are accepted by the tagger. These neural networks are trained and applied only to jets that are already tagged by the SECVTX algorithm. The current neural network b-tagging filter is tuned to increase the purity of the SECVTX b-tagged jets.

The neural networks take as input 16 variables chosen to distinguish b-quark jets from c- and l-quark jets by means of their higher track multiplicity, larger invariant mass, longer lifetime, and a harder fragmentation function than c- and l-quark jets. The track parameters and L_{xy} significance are good discriminators for b-jets. The sum of transverse momentum p_T^{vtx} and mass M_{vtx} of the tracks associated with the displaced vertex are useful variables for identifying l-jets; however c-jets have p_T spectra similar to b-jets. Pseudo-$c\tau$ ($L_{xy} \times M_{\text{vtx}}/p_T^{\text{vtx}}$), the vertex fit χ^2, and the track-based probability for a jet to originate away from the primary vertex are the best discriminators for b-jets.

The neural network b-tagging filter is validated by comparing the performance on a b-enriched sample of SECVTX tagged heavy-flavor jets from events with an electron candidate with $E_T > 8$ GeV and from the corresponding Monte Carlo sample. A good agreement is found in neural network b-tagging filter performance between data and Monte Carlo [7,8].

The output of the neural network is a value ranging from 0 to 1. We cut on this value so that we reject 65% of light-flavor jets and about 50% of the c jets while keeping 90% of b-jets which were tagged by SECVTX. The data-to-Monte-Carlo correction factor, measured from the electron sample, is 0.97 ± 0.02. Note that this is an additional correction factor with respect to the SECVTX efficiency scale factor because all of the jets under consideration have already been tagged by SECVTX.

C. Jet probability b-tagging

The jet probability b-tagging algorithm differs from SECVTX in that it employs the signed impact parameters (and their uncertainties) of all tracks within a jet and calculates the probability that the jet was produced at a position consistent with the primary vertex. The signed impact parameter of a track is defined as positive if the angle between the jet direction and the line joining the primary vertex to the point of closest approach of the track is less than 90 degrees, and it is defined as negative otherwise. A feature of this algorithm is that the b-tagging is performed using a continuous variable instead of a discrete object like a reconstructed secondary vertex.

For a light-quark jet, most particles should originate from the primary vertex. Because of the finite tracking resolution, charged particle tracks can be reconstructed with a nonzero impact parameter and have an equal probability to be either positively or negatively signed. Since a long-lived particle will travel some distance along the jet direction before decaying, its decay products will preferentially have positively signed impact parameters.

To calculate the track probability, the tracking resolution can be extracted by fitting the negative side of the signed

impact parameter distribution from the inclusive jet data which is dominated by prompt jets. Tracks are sorted into different categories (η, p_T of tracks, and quality of silicon detector hits) to parametrize their properties. To minimize the contribution from badly measured tracks with large reconstructed impact parameters, the distribution of a related quantity, the signed impact parameter significance (ratio of the signed impact parameter to its uncertainty) is parametrized for each track category. Each track is required to satisfy the quality criteria of $p_T > 0.5$ GeV$/c$ and a minimum number of hits in the tracking detector.

To calculate the jet probability from tracks, at least two tracks with positive impact parameter are required. By definition, the jet probability distribution should be flat between 0 and 1 for jets having only prompt tracks and peaked near zero for heavy-flavor jets having a large positively signed impact parameter. Tracks with a negative impact parameter are used to define a negative jet probability, which is used to check the algorithm and to estimate the misidentification rate. A jet is considered as tagged if the jet probability is less than 5%. We choose this value such that we reject 95% of light-flavor jets while keeping 60% of b-jets. The difference in efficiency between the simulated and observed data is taken into account as a scale factor. We measure the scale factor to be 0.85 ± 0.07 in a sample of high-E_T jets enriched in b jets by requiring a soft lepton from semileptonic heavy-flavor decay. A more detailed description of the scale factor estimation is given in Ref. [11].

V. BACKGROUND

The final state signature of $WH \rightarrow \ell\nu b\bar{b}$ production can be mimicked by other processes. The dominant background processes are W + jets production, $t\bar{t}$ production, and non-W QCD multijet production. Several electroweak production processes also contribute but with smaller rates. In the following subsections the contribution from each background source is discussed in detail. These background estimations are based on the same strategies used in the previous analysis [7,8]. The quantitative background estimates can be found in Sec. VIII.

A. Non-W QCD multijet

Events from QCD multijet production sometimes mimic the W-boson signature due to fake leptons and fake $\not\!\!E_T$. A non-W lepton is reconstructed when a jet passes the lepton selection criteria or a heavy-flavor jet produces leptons via semileptonic decay. Non-W $\not\!\!E_T$ can result from mismeasurements of energy or semileptonic decays of heavy-flavor quarks. Since the $\not\!\!E_T$ mismeasurement is usually not well modeled in detector simulation, we directly estimate the contribution of non-W events from the lepton + jets data before b-tagging is applied, known as the pretag sample.

Generally, the bulk of non-W events are characterized by a nonisolated lepton and small $\not\!\!E_T$. The lepton isolation I is defined as the ratio of the sum of the calorimeter energy inside a cone of $\Delta R = 0.4$ around the lepton direction, excluding the lepton energy, and the lepton energy itself. The quantity I is small if the lepton is well-isolated from the rest of the event, as typified by a true leptonic W decay. This feature is used to extrapolate the expected non-W contribution into our signal region, namely, small I and large $\not\!\!E_T$. In extracting the non-W background contribution from data, we make the following two assumptions: lepton isolation and $\not\!\!E_T$ are uncorrelated in non-W events, and the b-tagging rate is not dependent on $\not\!\!E_T$ in non-W events. The level at which these assumptions are justified determines the assigned uncertainty. The contributions from $t\bar{t}$ and W + jets events are subtracted according to the calculated cross sections for those processes.

To validate the method and estimate the relevant systematic uncertainties, we vary the boundaries of the signal and background regions. The observed deviations imply a 25% systematic uncertainty in the non-W background yield, assigned conservatively for both the pretag and tagged estimates [7,8].

The contribution of non-W background passing the NN b-tagging filter is determined by using data in the background region ($I > 0.2$ and $\not\!\!E_T > 20$ GeV), which has event kinematics similar to non-W events in the signal region because lepton isolation is the only difference between the two regions. The non-W estimate after applying the NN b-tagging filter is scaled by the ratio of the before NN b-tagging filter to the after NN b-tagging filter in this background region; this assumes the NN b-tagging filter is uncorrelated with the isolation.

The non-W estimate for events with at least two b-tags is obtained by measuring the ratio of the number of events with at least one b-tag to the number with at least two b-tags in the background region and applying the ratio to the estimate of tagged non-W events in the signal region.

For the plug region, the MET + PEM trigger is used, which means the above method is not valid, because of the $\not\!\!E_T$ trigger bias. The $\not\!\!E_T$ distribution shape difference between the non-W background and other backgrounds is therefore used to measure the amount of non-W background. To model the $\not\!\!E_T$ distribution shape in the non-W events, the control samples with electron candidates which failed at least two of our standard lepton identification criteria are used. We perform a likelihood fit of the $\not\!\!E_T$ distribution for observed data using the non-W and other background shapes [22].

B. W + mistagged jets

The rate at which SECVTX falsely tags light-flavor jets is derived from inclusive jet samples by counting the number of negative mistags. These are defined as jets tagged with an unphysical negative decay length, resulting from im-

perfect tracking resolution. They are assumed to be a good estimate of falsely tagged jets, independent to first order of heavy-flavor content in the generic jet sample and parametrized as a function of η, number of vertices, jet E_T, track multiplicity, z position of primary vertex, and total event E_T scalar sum. To estimate the positive mistag rate, the negative mistag rate is corrected for the enhancement of positive tags due to real secondary vertices in light-flavor jets and to interactions in the detector material. This factor is measured in an inclusive jet sample by fitting the asymmetry in the vertex mass distribution of positive tags over negative tags [25]. The systematic uncertainty on the mistag rate is estimated from the differences between observed and expected negative tags when applying the same parametrization to different jet samples.

The mistag rate per jet is applied to W + jets events. The total estimate is corrected for the non-W QCD fraction and also for the top-quark contributions to the pretag sample. To estimate the mistag contribution in NN-tagged events, we apply the light-flavor rejection factor of the NN filter 0.35 ± 0.05 as measured using light-flavor jets from various data and simulated samples. To estimate the mistag contribution in double tagged events, we apply the mistag rate to all untagged jets in $W + 1$ b-tagged jet events. This method accounts for the case of one real b-tag plus one mistag and also for the double-mistag case in which both b-tagged jets are not due to b-hadron decays.

For jet probability b-tagging, the mistag rate is derived from inclusive jet samples as a function of η, z position of the primary vertex, jet E_T, track multiplicity, number of vertices, and total event scalar E_T. The mistag rate probabilities are derived from jets with negatively signed impact parameters and applied in the same way as for the SECVTX algorithm [11].

C. W + heavy flavor

The $Wb\bar{b}$, $Wc\bar{c}$, and Wc processes are major background sources after the requirement of b-tagging. Large theoretical uncertainties exist for the overall normalization because current Monte Carlo event generators can generate W + heavy-flavor events only to leading order. Consequently, the rates for these processes are normalized to data. The contribution from true heavy-flavor production in W + jets events is determined from measurements of the heavy-flavor event fraction in W + jets events and the b-tagging efficiency for those events, as explained below.

The fraction of W + jets events produced with heavy-flavor jets has been studied extensively using an alpgen + pythia combination of Monte Carlo simulations [26,27]. Calculations of the heavy-flavor fraction in ALPGEN have been calibrated using a jet data sample, and measurements indicate that a scaling factor of 1.4 ± 0.4 is necessary to make the heavy-flavor production in Monte Carlo match the production in $W + 1$ jet events. The final results obtained for heavy-flavor fractions are shown in Table I.

TABLE I. The heavy-flavor fractions f_{HF}, given in percent, for the W + jets events where $1B$, $2B$ refer to number of taggable b-jets in the events, with $1C$, $2C$ for charm jets. The results from ALPGEN Monte Carlo have been scaled by the data-derived calibration factor of 1.4 ± 0.4.

Jet Multiplicity	1 jet	2 jets	3 jets	≥ 4 jets
$Wb\bar{b}$ (1B) (%)	1.0 ± 0.4	2.0 ± 0.8	3.4 ± 1.4	4.6 ± 2.0
$Wb\bar{b}$ (2B) (%)	...	1.3 ± 0.6	2.5 ± 1.0	3.1 ± 1.8
$Wc\bar{c}$ (1C) (%)	7.7 ± 2.4	12.2 ± 4.5	16.4 ± 5.3	18.6 ± 6.9
$Wc\bar{c}$ (2C) (%)	...	2.0 ± 0.8	4.6 ± 1.8	8.4 ± 3.4

For the tagged W + heavy flavor (HF) background estimate, the heavy-flavor fractions and tagging rates given in Tables I and II are multiplied by the number of pretag W + jets candidate events (N_{pretag}) in data, after correction for the contribution of non-W ($f_{\mathrm{non}-W}$), $t\bar{t}$ and other background events to the pretag sample. The W + heavy flavor background contribution is obtained by the following relation:

$$N_{W+\mathrm{HF}} = f_{\mathrm{HF}} \cdot \epsilon_{\mathrm{tag}} \cdot [N_{\mathrm{pretag}} \cdot (1 - f_{\mathrm{non}-W}) - N_{\mathrm{TOP}} - N_{\mathrm{EWK}}], \quad (4)$$

where f_{HF} is the heavy-flavor fraction, ϵ_{tag} is the tagging efficiency, N_{TOP} is the expected number of $t\bar{t}$ and single top events, and N_{EWK} is the expected background contribution from WW, WZ, ZZ and Z boson events.

D. Top and electroweak backgrounds

Production of both single top quarks and top-quark pairs contributes to the tagged W + jets sample. Several electroweak boson production processes also contribute. WW pairs can decay to a lepton, neutrino as missing energy, and two jets, one of which may be charm. WZ events can decay

TABLE II. The b-tagging efficiencies ϵ_{tag} in percent for the various b-tagging strategies on individual W + heavy-flavor processes. Categories $1B$, $2B$ refer to number of taggable b-jets in the events, with similar categories for charm jets. Those numbers include the effect of the data-to-Monte Carlo scale factors.

Jet Multiplicity	1 jet	2 jets	3 jets	≥ 4 jets
1 SECVTX and NN b-tag (%)				
$Wb\bar{b}$ (1B)	27.5 ± 1.5	28.1 ± 1.3	26.7 ± 1.4	26.9 ± 3.7
$Wb\bar{b}$ (2B)	...	26.2 ± 1.2	24.1 ± 1.2	22.6 ± 1.3
$Wc\bar{c}$ (1C)	4.2 ± 0.2	4.6 ± 0.3	4.9 ± 0.3	5.2 ± 0.7
$Wc\bar{c}$ (2C)	...	6.3 ± 0.4	6.6 ± 0.4	6.9 ± 0.6
≥ 2 secvtx b-tag (%)				
$Wb\bar{b}$ (2B)	...	16 ± 2	19 ± 2	19 ± 3
$Wc\bar{c}$ (2C)	...	1.0 ± 0.5	2.0 ± 1.0	2.0 ± 1.0
1 secvtx + Jet Probability b-tag (%)				
$Wb\bar{b}$ (2B)	...	10.1 ± 1.2	11.1 ± 1.3	12.4 ± 1.5
$Wc\bar{c}$ (2C)	...	1.6 ± 0.2	2.3 ± 0.3	3.2 ± 0.4

TABLE III. Theoretical cross sections and uncertainties for the electroweak and single top backgrounds, along with the theoretical cross section for $t\bar{t}$ at $m_t = 175$ GeV/c^2 [28]. The cross section of $Z^0 \to \tau^+\tau^-$ is obtained in the dilepton mass range $m_{\tau\tau} > 30$ GeV/c^2 together with a k-factor (NLO/LO) of 1.4 [29].

Background	Theoretical Cross Sections
WW	12.40 ± 0.25 pb
WZ	3.96 ± 0.06 pb
ZZ	1.58 ± 0.05 pb
Single top s-channel	0.88 ± 0.11 pb
Single top t-channel	1.98 ± 0.25 pb
$Z \to \tau^+\tau^-$	265 ± 30.0 pb
$t\bar{t}$	$6.7^{+0.7}_{-0.9}$ pb

to the signal $\ell\nu b\bar{b}$ or $\ell\nu c\bar{c}$ final state. Finally, $Z \to \tau^+\tau^-$ events can have one leptonic τ decay and one hadronic decay. The leptonic τ decay gives rise to a lepton plus missing transverse energy, while the hadronic decay yields a narrow jet of hadrons with a nonzero lifetime.

The normalization of the diboson and top production backgrounds are based on the theoretical cross sections listed in Table III, the luminosity, and the acceptance and b-tagging efficiency derived from Monte Carlo events [21,30–32]. The acceptance is corrected for lepton identification, trigger efficiencies, and the z vertex cut. The tagging efficiency is corrected by the b-tagging scale factor.

VI. HIGGS BOSON SIGNAL ACCEPTANCE

The PYTHIA Monte Carlo generator is used to generate the signal samples and study the kinematic properties [33]. Only Higgs boson masses between 110 and 150 GeV/c^2 are considered because this is the mass region, especially up to 135 GeV/c^2, for which the decay $H \to b\bar{b}$ dominates. The number of expected $WH \to \ell\nu b\bar{b}$ events N is given by

$$N = \epsilon \cdot \int \mathcal{L}dt \cdot \sigma(p\bar{p} \to WH) \cdot \mathcal{B}(H \to b\bar{b}), \quad (5)$$

where ϵ, $\int \mathcal{L}dt$, $\sigma(p\bar{p} \to WH)$, and $\mathcal{B}(H \to b\bar{b})$ are the event detection acceptance, integrated luminosity, production cross section, and branching fraction, respectively. The production cross section and branching fraction are calculated to NLO precision [5]. The acceptance ϵ is broken down into the following factors:

$$\epsilon = \epsilon_{z_0} \cdot \epsilon_{b\text{tag}} \cdot \sum_{\ell=e,\mu,\tau} (\epsilon_{\text{trigger}} \cdot \epsilon_{\text{lepton ID}} \cdot \epsilon_{\text{kinematics}} \cdot \mathcal{B}(W \to \ell\nu)), \quad (6)$$

where ϵ_{z_0}, $\epsilon_{\text{trigger}}$, $\epsilon_{\text{lepton ID}}$, $\epsilon_{b\text{tag}}$, and $\epsilon_{\text{kinematics}}$ are efficiencies defined in sequence to meet the requirements of primary vertex, trigger, lepton identification, b-tagging, and event selection criteria. The major sources of inefficiency are the lepton identification, jet kinematics, and b-tagging factors; each has an efficiency between 30 and 45%. The factor ϵ_{z_0} is obtained using the vertex distribution from the minimum bias data, $\epsilon_{\text{trigger}}$ is measured using a clean $W \to l\nu$ data sample, obtained from different triggers after applying more stringent offline cuts, and $\epsilon_{\text{lepton ID}}$ is calculated using $Z \to ll$ observed data and Monte Carlo samples. $\epsilon_{b\text{tag}}$ is measured in a b-enriched sample from semileptonic heavy-flavor decay. The total signal acceptances are shown in Fig. 1 for the selected b-tagging options as a function of Higgs boson mass. Inclusion of forward electrons in this analysis increased the overall acceptance by 10%.

The total systematic uncertainty on the acceptance stems from the jet energy scale, initial and final state radiation (ISR and FSR), lepton identification, trigger efficiencies, and b-tagging scale factor. A 2% uncertainty on the lepton identification efficiency is assigned for each lepton type (CEM electron, PEM electron, CMUP and CMX muon), based on studies of Z boson events. For each of the high p_T lepton triggers, a 1% uncertainty is measured from backup trigger paths or Z boson events.

The initial and final state radiation systematic uncertainties are estimated by changing the parameters in the Monte Carlo related to ISR and FSR from nominal values to half or double the nominal [34]. Half of the difference from the two samples is taken as the systematic uncertainty. The uncertainty in the incoming parton energies relies on the eigenvectors provided in the PDF fits. A NLO version of the PDFs, CTEQ6M, provides a 90% confidence interval of each eigenvector [35]. The nominal PDF value is reweighted to the 90% confidence level value, and the corresponding reweighted acceptance is computed.

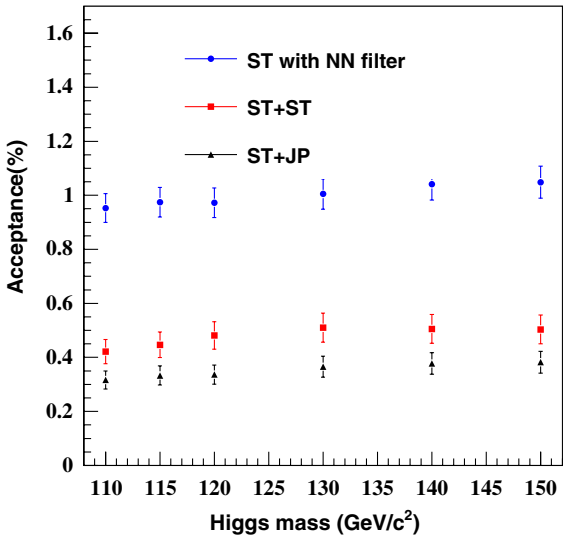

FIG. 1 (color online). The total acceptance ϵ for the process $WH \to \ell\nu b\bar{b}$ in $W + 2$ jet bin for the selected b-tagging strategies as a function of Higgs boson mass.

TABLE IV. Systematic uncertainties on signal acceptance for the selected b-tagging requirements.

b-tagging category	LeptonID	Trigger	ISR/FSR	JES	PDF	b-tagging	Total
ST with NN filter	~2%	<1%	2.9%	2.3%	1.2%	3.5%	5.6%
ST + ST	~2%	<1%	5.2%	2.5%	2.1%	8.4%	10.6%
ST + JP	~2%	<1%	4.0%	2.8%	1.5%	9.1%	10.5%

The differences between nominal and reweighted acceptances are added in quadrature, and the total is assigned as the systematic uncertainty [10].

The effect of the jet energy scale uncertainty (JES) [17] is calculated by shifting the jet energy scale by $\pm 1\sigma$ in the WH Monte Carlo samples. The deviation from the nominal acceptance is taken as the systematic uncertainty. The systematic uncertainty on the b-tagging efficiency is based on the scale factor uncertainty discussed in Secs. IV A and IV C. When the NN b-tagging filter is applied, the scale factor uncertainty is added to that of SECVTX in quadrature. The total systematic uncertainties for the selected b-tagging options are summarized in Table IV.

The expected number of signal events is estimated by Eq. (5) at each Higgs boson mass point. The expectations for the selected b-tagging strategies are shown in Table V.

VII. NEURAL NETWORK DISCRIMINANT

To further improve the signal to background discrimination after event selection, we employ a neural network [24] trained on a variety of kinematic variables to distinguish the W + Higgs events from the backgrounds.

The neural network on the samples of simulated events using a mixture of 50% signal and 50% of backgrounds is trained. The background composition is chosen to have equal amounts of $Wb\bar{b}$, $t\bar{t}$, and single top, which provides a maximum sensitivity over a wide range of input conditions.

To optimize the neural network structure, we use an iterative procedure to determine the configuration that best discriminates signal from the background, and uses a minimal number of input discriminants. This is done by first determining the best one-variable neural network from a list of 76 possible variables, based on the kinematic distributions of the two jets, lepton, and $\not\!\!E_T$ in the events (including correlations among these objects). The optimization algorithm keeps this variable as an input and then loops over all other variables to determine the best two-variable neural network. The best N-variable neural network is finally selected once the $(N+1)$-variable neural network shows less than 0.5% improvement. The criteria for comparing neural networks is the testing error defined by how often a neural network with a given configuration incorrectly classifies signal and background events. This optimization of the neural network structure was done for Higgs mass of 120 GeV/c^2, and we use the same structure to train separate neural networks for Higgs masses of 110, 115, 120, 130, 140, and 150 GeV/c^2. Retraining neural networks with different signal masses keeps the neural network improvement almost constant as a function of the Higgs mass.

Our neural network configuration has 6 input variables, 11 hidden nodes, and 1 output node. The output of the neural network has a value from 0 to 1 that will provide discrimination between the signal and background hypotheses. The signal-like events yield a high neural network value and the background like events yield a low neural network value.

The 6 optimal inputs are as follows:

(i) M_{jj+}: the invariant mass calculated from the two jets in the $W+2$ jets event. Furthermore, if there are additional loose jets present, the loose jet that is closest to one of the two jets is included in this invariant mass calculation, if the separation between that loose jet and one of the jets is $\Delta R < 0.9$. This definition gives greater discriminating power for instances where the selected b-jet spreads outside the cone.

(ii) $\sum E_T$ (Loose Jets): the scalar sum of the transverse energies of the loose jets.

(iii) p_T Imbalance: the difference between the scalar sum of the transverse momenta of all measured objects and the $\not\!\!E_T$. Specifically, it is calculated as $P_T(\text{jet}_1) + P_T(\text{jet}_2) + P_T(\text{lep}) - \not\!\!E_T$.

(iv) $M_{l\nu j}^{\min}$: the invariant mass of the lepton, $\not\!\!E_T$, and one of the two jets, where the jet is chosen to give the

TABLE V. Expected number of $WH \to \ell\nu b\bar{b}$ signal events in central region for the selected b-tagging options. All systematic uncertainties are included.

b-tagging category	110 GeV	115 GeV	120 GeV	130 GeV	140 GeV	150 GeV
Pretag	9.41 ± 0.61	7.92 ± 0.52	6.35 ± 0.41	3.99 ± 0.26	2.02 ± 0.13	0.78 ± 0.05
ST with NN filter	2.63 ± 0.22	2.20 ± 0.18	1.70 ± 0.14	1.08 ± 0.09	0.55 ± 0.05	0.21 ± 0.02
ST + ST	1.18 ± 0.14	1.00 ± 0.12	0.85 ± 0.10	0.55 ± 0.07	0.27 ± 0.03	0.10 ± 0.01
ST + JP	0.89 ± 0.11	0.76 ± 0.09	0.60 ± 0.07	0.40 ± 0.05	0.20 ± 0.02	0.08 ± 0.01

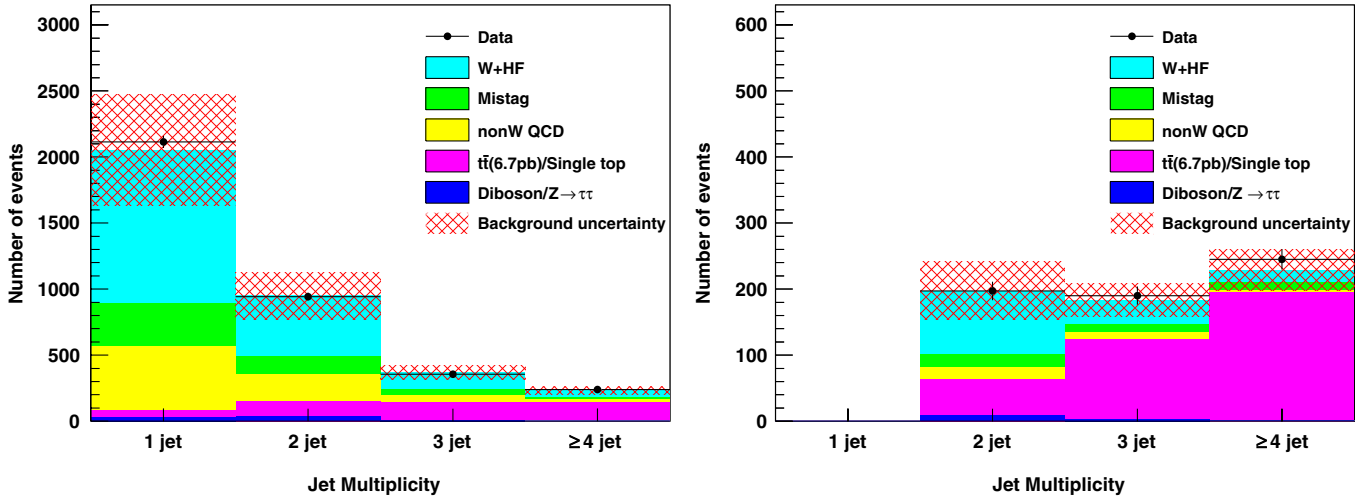

FIG. 2 (color online). Number of events in the central and plug regions are shown as a function of jet multiplicity for events with exactly one SECVTX b-tag applying the NN b-tagging filter (left) and for events with at least two SECVTX b-tagged jets or one SECVTX b-tagged jet plus one jet probability b-tagged jet (right).

minimum invariant mass. For this quantity, the p_z component of the neutrino is ignored.

(v) ΔR (lepton-$\nu_{\max}$): the ΔR separation between the lepton and the neutrino, where the p_z of the neutrino is taken by choosing the largest $|p_z|$ of solutions from the quadratic equations for the W mass (80.42 GeV$/c^2$) constraint.

(vi) $P_T(W + H)$: the norm of the vector sum of transverse momentum of the lepton, $\not\!\!E_T$ and two jets.

Distributions of all these quantities are checked for both the pretag and tagged samples. The simulated background events match to the real data well.

VIII. RESULTS

A. Counting results

The observed number of events in data is compared to the expected background in Fig. 2, as a function of jet multiplicity. Results are shown for the single and double b-tagged categories separately. Table VI shows the composition of $W + 2$ jet data in each b-tagging category and in the central lepton and plug lepton regions, respectively.

The observed number of events in the data and the standard model background expectations are consistent in each b-tagging category.

TABLE VI. Predicted sample composition and observed number of $W + 2$ jet events in the central and plug regions with the selected b-tagging options.

	Central region			Plug region		
Pretag Events	32242			5879		
b-tagging	ST + ST	ST + JP	ST + NN	ST + ST	ST + JP	ST + NN
Mistag	3.88 ± 0.35	11.73 ± 0.92	107.1 ± 9.38	1.00 ± 0.18	3.18 ± 0.49	28.47 ± 3.30
$Wb\bar{b}$	37.93 ± 16.92	31.15 ± 14.03	215.6 ± 92.34	7.40 ± 3.96	6.23 ± 3.37	43.09 ± 12.33
$Wc\bar{c}$	2.88 ± 1.25	7.87 ± 3.43	167.0 ± 62.14	0.96 ± 0.49	1.53 ± 0.81	33.37 ± 9.55
$t\bar{t}$ (6.7 pb)	19.05 ± 2.92	15.56 ± 2.39	60.68 ± 9.30	2.14 ± 0.34	1.79 ± 0.31	7.17 ± 1.00
Single top(s-ch)	6.90 ± 1.00	5.14 ± 0.75	14.38 ± 2.09	0.69 ± 0.10	0.51 ± 0.08	1.53 ± 0.20
Single top(t-ch)	1.60 ± 0.23	1.87 ± 0.27	29.57 ± 4.33	0.22 ± 0.04	0.24 ± 0.04	3.54 ± 0.47
WW	0.17 ± 0.02	0.93 ± 0.11	15.45 ± 1.91	0.01 ± 0.01	0.12 ± 0.04	3.00 ± 0.20
WZ	2.41 ± 0.26	1.84 ± 0.20	7.59 ± 0.81	0.58 ± 0.06	0.42 ± 0.05	1.62 ± 0.09
ZZ	0.06 ± 0.01	0.08 ± 0.01	0.31 ± 0.03	0.00 ± 0.01	0.01 ± 0.01	0.02 ± 0.00
$Z \to \tau\tau$	0.25 ± 0.04	1.29 ± 0.20	7.27 ± 1.12	0.00 ± 0.01	0.01 ± 0.01	0.24 ± 0.03
Non-W QCD	5.50 ± 1.00	9.55 ± 1.73	184.7 ± 33.04	1.16 ± 0.44	1.51 ± 0.55	18.34 ± 5.54
Total Background	80.6 ± 18.8	87.0 ± 18.0	809.6 ± 159.4	14.2 ± 4.0	15.5 ± 3.6	140.4 ± 16.9
WH signal (120 GeV)	0.85 ± 0.10	0.60 ± 0.07	1.70 ± 0.14	0.09 ± 0.01	0.06 ± 0.01	0.20 ± 0.01
Observed Events	83	90	805	11	13	138

B. Limit on Higgs boson production rate

We apply the neural network discriminant discussed in the previous section to the samples of simulated events and obtain the distributions of the network output for all the processes considered. The expected distributions are compared to the data observed in single and double b-tagged categories as shown in Fig. 3. We use a binned likelihood technique to fit the observed neural network output distributions in the three b-tagging categories to test for the presence of a WH signal.

The number of events in each bin follows the Poisson distribution

$$P_i(n_i, \mu_i) = \frac{\mu_i^{n_i} e^{-\mu_i}}{n_i!} \qquad (i = 1, 2, \cdots, N_{\text{bin}}), \quad (7)$$

where n_i, μ_i, and N_{bin} represent the number of observed events in the i-th bin, the expectation in the i-th bin, and the total number of bins. The Higgs production hypothesis is constructed by setting μ_i to $\mu_i = s_i + b_i$, where s_i and b_i are the number of signal and expected background events in the i-th bin. This quantity s_i can also be written as a product

$$s_i = \sigma(p\bar{p} \to W^{\pm}H) \cdot \mathcal{B}(H \to b\bar{b}) \cdot \epsilon \cdot \int \mathcal{L}dt \cdot f_i^{WH}, \quad (8)$$

where f_i^{WH} is the fraction of the total signal which lies in the i-th bin. In this case, $\sigma(p\bar{p} \to W^{\pm}H) \cdot \mathcal{B}(H \to b\bar{b})$ is the variable to be extracted from data. The likelihoods from the three b-tagging categories are multiplied together. The systematic uncertainties associated with the pretag acceptance, luminosity, and the b-tagging efficiency scale factor are considered to be fully correlated among the three selection categories. Background uncertainties on the heavy-flavor fractions are completely correlated among W + HF backgrounds, and background uncertainties on b-tagging scale factor are also completely correlated among all backgrounds. The systematic uncertainties associated with the shape of network output are also studied and found to have a negligible impact on the final results.

Since we observe no excess over the background prediction, an upper limit on the Higgs boson production cross section times branching fraction $\sigma(p\bar{p} \to W^{\pm}H) \cdot \mathcal{B}(H \to b\bar{b})$ is extracted by using a Bayesian procedure. We assume a uniform prior probability for $\sigma \cdot \mathcal{B}$ and integrate the likelihood over all parameters except for $\sigma \cdot \mathcal{B}$. The 95% confidence level upper limits on $\sigma \cdot \mathcal{B}$ are obtained by calculating the 95th percentile of the resulting distributions.

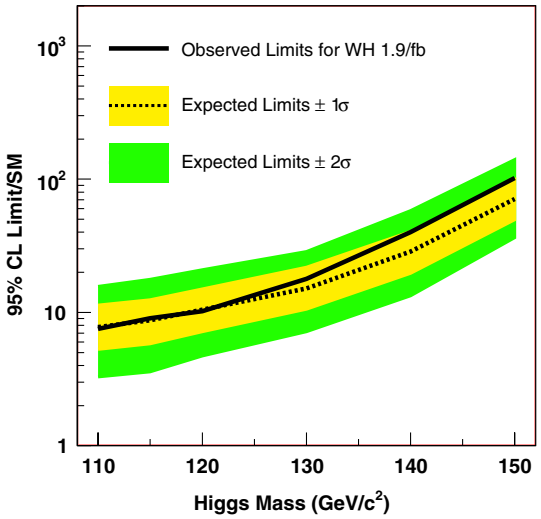

FIG. 4 (color online). The observed (solid) and expected (dashed) 95% confidence level upper limit on $\sigma(p\bar{p} \to WH) \cdot \mathcal{B}(H \to b\bar{b})$ relative to the standard model expectations with an integrated luminosity of 1.9 fb^{-1} along with the one and two σ bands of the distributions of expected outcomes from pseudoexperiments.

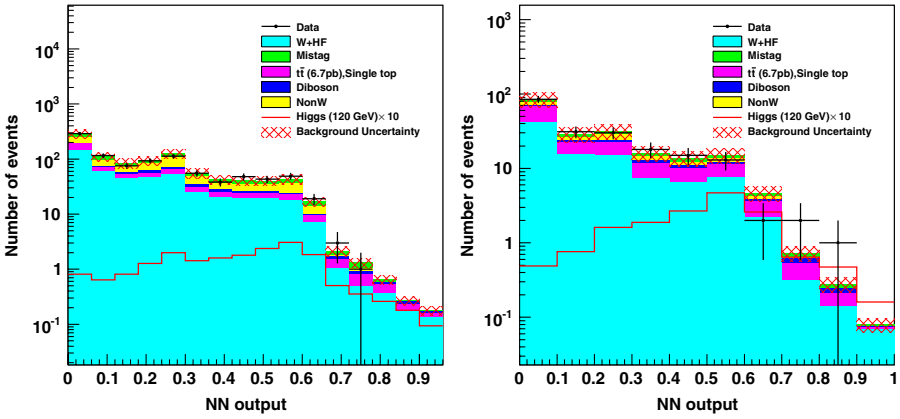

FIG. 3 (color online). Neural Network output distribution in W + 2 jets events for exactly one SECVTX b-tagged jet that passes the NN b-tagging filter (left) and events for ST + ST and ST + JP double b-tagging categories (right). The contributions of the various background sources from the central plus plug region are shown in histograms while the hatched box represents the background uncertainty. The expected signal for a 120 GeV Higgs boson (multiplied by a factor of 10) is shown by the solid line.

TABLE VII. Observed and expected upper limits on $\sigma(p\bar{p} \to WH) \cdot \mathcal{B}(H \to b\bar{b})$ at 95% C.L. compared to the standard model production rate calculated at NLO.

Higgs Mass	Upper Limit (pb)		Upper Limit/SM	
GeV/c^2	Observed	Expected	Observed	Expected
110	1.2	1.2	7.5	7.8
115	1.2	1.1	9.0	8.7
120	1.1	1.1	10.2	10.5
130	1.1	0.9	17.9	15.2
140	1.2	0.8	40.1	28.7
150	1.1	0.8	101.9	70.9

To evaluate the sensitivity of the analysis, background-only pseudoexperiments are used to calculate the expected limit in the absence of Higgs boson production. Pseudo data are generated by fluctuating the individual background estimates within their total uncertainties. The expected limit is defined as the median of the 95% confidence level upper limits of 1000 pseudoexperiments.

The observed limits as a function of the Higgs boson mass are shown in Fig. 4 and Table VII, together with the expected limits determined from pseudoexperiments. We set 95% confidence level upper limits on the production cross section times branching fraction ranging from 1.2 to 1.1 pb or 7.5 to 101.9 times the standard model expectation for Higgs boson masses from 110 to 150 GeV/c^2, respectively.

IX. CONCLUSIONS

We have presented a search for the standard model Higgs boson in the $\ell\nu b\bar{b}$ final state expected from WH production at CDF. The search sensitivity is improved significantly with respect to previous searches, by about 60% more than the expectation from simple luminosity scaling. The main improvements are using jet probability b-tagging, a multivariate neural network technique to further enhance sensitivity to the signal, and increasing the acceptance for signal events by including leptons in the forward region of the detector. These improvements, along with a data set of 1.9 fb^{-1}, allow us to set a 95% confidence level upper limit on the production cross section times branching fraction that ranges from 1.2 to 1.1 pb or 7.5 to 101.9 times the standard model expectation for Higgs boson masses spanning from 110 to 150 GeV/c^2, respectively.

This channel is an important component of the combined search for the Higgs boson at the Tevatron [36]. With the Tevatron expected to deliver a factor of 4 more data, it is possible that the combined search with the complete data set will be sensitive to the standard model Higgs cross section in this low mass range, which is of particular interest according to indications derived from standard model fits to electroweak observables [3].

ACKNOWLEDGMENTS

We thank the Fermilab staff and the technical staffs of the participating institutions for their vital contributions. This work was supported by the U.S. Department of Energy and National Science Foundation; the Italian Istituto Nazionale di Fisica Nucleare; the Ministry of Education, Culture, Sports, Science and Technology of Japan; the Natural Sciences and Engineering Research Council of Canada; the National Science Council of the Republic of China; the Swiss National Science Foundation; the A. P. Sloan Foundation; the Bundesministerium für Bildung und Forschung, Germany; the Korean Science and Engineering Foundation and the Korean Research Foundation; the Science and Technology Facilities Council and the Royal Society, UK; the Institut National de Physique Nucleaire et Physique des Particules/CNRS; the Russian Foundation for Basic Research; the Ministerio de Ciencia e Innovación, and Programa Consolider-Ingenio 2010, Spain; the Slovak R&D Agency; and the Academy of Finland.

[1] P. W. Higgs, Phys. Rev. Lett. **13**, 508 (1964).
[2] R. Barate *et al.* (ALEPH, DELPHI, L3, OPAL Collaborations, and LEP Working Group for Higgs Boson Searches), Phys. Lett. B **565**, 61 (2003).
[3] LEP-Tevatron-SLD Electroweak Working Group, arXiv:0811.4682.
[4] T. Han and S. Willenbrock, Phys. Lett. B **273**, 167 (1991).
[5] A. Djouadi, J. Kalinowski, and M. Spira, Comput. Phys. Commun. **108**, 56 (1998).
[6] A. Abulencia *et al.* (CDF Collaboration), Phys. Rev. D **75**, 012010 (2007).
[7] T. Aaltonen *et al.* (CDF Collaboration), Phys. Rev. Lett. **100**, 041801 (2008).
[8] T. Aaltonen *et al.* (CDF Collaboration), Phys. Rev. D **78**, 032008 (2008).
[9] V. M. Abazov *et al.* (D0 Collaboration), Phys. Lett. B **663**, 26 (2008).
[10] D. Acosta *et al.* (CDF Collaboration), Phys. Rev. D **71**, 052003 (2005).
[11] A. Abulencia *et al.* (CDF Collaboration), Phys. Rev. D **74**, 072006 (2006).
[12] D. Acosta *et al.* (CDF Collaboration), Phys. Rev. D **71**, 032001 (2005).
[13] L. Balka *et al.*, Nucl. Instrum. Methods Phys. Res., Sect. A **267**, 272 (1988).
[14] S. Bertolucci *et al.*, Nucl. Instrum. Methods Phys. Res.,

Sect. A **267**, 301 (1988).
[15] M. G. Albrow *et al.*, Nucl. Instrum. Methods Phys. Res., Sect. A **480**, 524 (2002).
[16] F. Abe *et al.* (CDF Collaboration), Phys. Rev. D **45**, 1448 (1992).
[17] A. Bhatti *et al.*, Nucl. Instrum. Methods Phys. Res., Sect. A **566**, 375 (2006).
[18] G. Ascoli *et al.*, Nucl. Instrum. Methods Phys. Res., Sect. A **268**, 33 (1988).
[19] T. Dorigo (CDF Collaboration), Nucl. Instrum. Methods Phys. Res., Sect. A **461**, 560 (2001).
[20] E. J. Thomson *et al.*, IEEE Trans. Nucl. Sci. **49**, 1063 (2002).
[21] D. Acosta *et al.* (CDF Collaboration), Phys. Rev. Lett. **94**, 091803 (2005).
[22] T. Peiffer, Report No. FERMILAB-MASTERS-2008-01, 2008.
[23] A. Abulencia *et al.* (CDF Collaboration), Phys. Rev. Lett. **97**, 082004 (2006).
[24] C. Peterson, T. Rögnvaldsson, and L. Lönnblad, Comput. Phys. Commun. **81**, 185 (1994).
[25] A. Abulencia *et al.* (CDF Collaboration), Phys. Rev. Lett. **97**, 082004 (2006).
[26] M. L. Mangano, M. Moretti, F. Piccinini, R. Pittau, and A. D. Polosa, J. High Energy Phys. 07 (2003) 001.
[27] G. Corcella *et al.*, arXiv:hep-ph/0201201.
[28] S. Eidelman *et al.* (Particle Data Group), Phys. Lett. B **592**, 1 (2004).
[29] A. Abulencia *et al.* (CDF Collaboration), Phys. Rev. D **75**, 092004 (2007).
[30] J. Campbell and R. K. Ellis, Phys. Rev. D **65**, 113007 (2002).
[31] M. Cacciari, S. Frixione, M. L. Mangano, P. Nason, and G. Ridolfi, J. High Energy Phys. 04 (2004) 068.
[32] B. W. Harris, E. Laenen, L. Phaf, Z. Sullivan, and S. Weinzierl, Phys. Rev. D **66**, 054024 (2002).
[33] T. Sjöstrand *et al.*, Comput. Phys. Commun. **135**, 238 (2001).
[34] A. Abulencia *et al.* (CDF Collaboration), Phys. Rev. D **73**, 032003 (2006).
[35] J. Pumplin *et al.*, J. High Energy Phys. 07 (2002) 012.
[36] The Tevatron Working Group (CDF and D0 Collaborations), Report No. FERMILAB-PUB-08-069-E, 2008.